Highly stable PEDOT:PSS electrochemical transistors

Sophia L Bidinger,[a] Sanggil Han,[a] George G Malliaras,[b] and Tawfique Hasan[b]

Electrical Engineering Division, Department of Engineering, University of Cambridge, 9 JJ Thompson Ave, Cambridge CB3 0FA, UK

Organic electrochemical transistors (OECTs) are a burgeoning biosensing transducer platform due to their intrinsic amplification, high transconductance, and biocompatibility. To be successful in real world biosensing applications, however, stable performance should be demonstrated to avoid false analyte readings that could lead to dangerous misdiagnosis. This work demonstrates the stability of carefully prepared OECTs using commercially available PEDOT:PSS as the channel layer. These devices exhibit more than 99% retention of the baseline current over 50 transfer curve cycles and, importantly, after several changes of electrolyte solution. Furthermore, impressive stability is demonstrated during continuous measurements of the drain current. These results show that PEDOT:PSS OECTs are ready for biosensing applications requiring accurate continuous monitoring.

Organic electrochemical transistors (OECTs) have been attracting a great deal of attention for biosensing applications due to their high transconductance, biocompatibility, and facile integration with biological systems.[1–3] In particular, high transconductance is related to high sensitivity of sensors as the power of an input signal at the gate is amplified by a factor determined by the transconductance, $g_m = \partial I_D / \partial V_G$, where I_D and V_G denote the drain current and gate voltage, respectively.[2] Contrary to conventional field-effect transistors, where changes in channel conductivity only occur in a thin interfacial region, OECTs allow doping changes to take place throughout the entire volume of the channel.[4] This leads to exceptionally high g_m, and thus makes OECTs excellent amplifying transducers.[1–5] Poly(3,4ethylenedioxythiophene) doped with poly(styrene sulfonate) (PEDOT:PSS) is the most popular material as a channel layer of OECTs mainly due to its commercial availability and good material stability in an aqueous environment.[4,6] PEDOT:PSS films can be made insoluble in aqueous solutions by crosslinking them with (3-glycidyloxypropyl)trimethoxysilane (GOPS)[7] or divinylsulfone.[8] OECTs have been widely leveraged to develop a host of biosensors for detecting, for example, ions[9,10], metabolites[11–14], and viruses[15,16] with the aim of deploying them in the field or translating them to the clinic.

For OECT-based biosensors, there are two most common ways to measure analyte concentrations: via shifts in the transfer curves (i.e. discrete monitoring) or by recording changes in I_D in real time (i.e. continuous monitoring). Specifically, recognition elements such as ion selective membranes[9], enzymes[11–14], and aptamers[17,18] are attached onto

---

[a] These authors contributed equally to this work

[b] **Authors to whom correspondence should be addressed:** gm603@cam.ac.uk and th270@cam.ac.uk

the gate electrode or the channel. Upon interaction with an analyte, the recognition elements change the effective gate bias, which translates to changes in the transfer curve and the I_D. The former method involves repetitive measurement of the transfer curves (I_D - V_G) at a fixed drain voltage (V_D) while changing analyte solutions[17–19], which can be used for point-of-care *in vitro* testing, for example, rapid COVID tests.[16] This method requires high sensor cyclability (i.e. repeatability of transfer curves) to enable accurate measurements. The latter method involves continuous measurement of I_D in real time at fixed V_G and V_D.[9,11–13] This requires a stable baseline current to allow for real-time *in-vivo* testing, such as in wearables.[20]

Good stability has been demonstrated in OECTs made of a novel donor-acceptor conjugated polymer[21], however, this material is not commercially available. PEDOT:PSS OECTs, on the other hand, were shown to be stable only when the channel was crystalized through post-deposition treatment in concentrated sulfuric acid.[22] Although these results are significant, the added fabrication complexity and need to carefully control the crystallinity of the material may hinder translation. Here, we demonstrate that OECTs made with the "standard" recipe using the commercially available PEDOT:PSS dispersion are stable, with more than 99% current retention in both cycling of transfer curves and continuous I_D measurements. These results pave the way for deployment of OECTs in a broad range of biosensing applications.

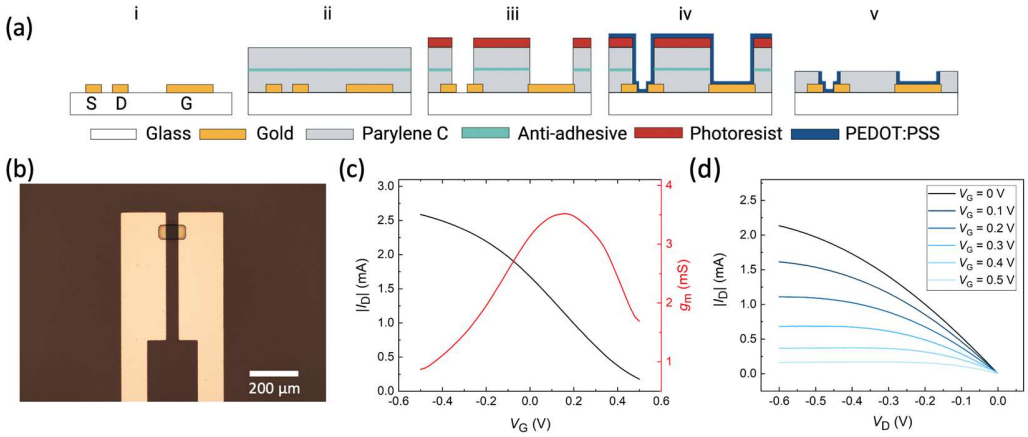

FIG. 1. (a) Schematic of the microfabrication steps showing formation of source (S), drain (D), and gate (G) electrodes (i), parylene-C deposition (ii) and etching (iii), PEDOT:PSS coating (iv), and peel-off (v) of the sacrificial parylene-C layer. Figure not drawn to scale. (b) Optical micrograph of a microfabricated OECT channel with source and drain electrodes (c) Transfer curve and transconductance of an OECT operated with a Ag/AgCl gate at a fixed V_D of -0.4 V exhibiting an I_D ON/OFF ratio of 63,500 (d) Output curves of an OECT gated with non-polarizable Ag/AgCl.

Ethylene glycol, 4-dodecylbenzenesulfonic acid (DBSA), and (3glycidyloxypropyl)trimethoxysilane (GOPS) were purchased from Sigma-Aldrich. 3-(trimethoxysilyl)propyl methacrylate (Silane A174) was purchased from Thermo Fisher Scientific. PEDOT:PSS (Clevios PH1000) was purchased from Heraeus. A careful microfabrication process was performed based on previously published protocol[23] as illustrated in Fig. 1(a). First, source, drain, and planar gate electrodes and interconnects were defined on glass substrates using AZnLOF 2035 (Microchemicals GmbH) negative photoresist. Following lithography, samples were activated for gold adhesion with one minute of oxygen plasma (Diener Electronic Femto). Next, 5 nm of titanium and 100 nm of gold were deposited using an e-beam evaporator (Kurt J Lesker PVD-75). After deposition, liftoff (step i) was performed by acetone and isopropyl alcohol (IPA). Samples were then silane treated for adhesion to the first parylene-C (PaC). Next, two separate layers of 2 μm thick PaC were deposited (step ii). Between the two layers, a 2% micro-90 solution diluted with deionized (DI) water was spin-coated as an anti-adhesive layer for peel-off. AZ 10XT (Microchemicals GmbH), a positive photoresist, was used for the second lithography step. After this, channel, gate, and contact pad areas were formed by etching PaC using a reactive ion etcher (Oxford 80 Plasmalab plus), shown in step iii. Next, 5% (v/v) ethylene glycol and 0.25% (v/v) DBSA were mixed with PEDOT:PSS by sonication. 1% (v/v) GOPS was added to the PEDOT:PSS blend and filtered using a 0.45 μm polytetrafluoroethylene filter. The samples were treated with oxygen plasma to produce hydroxyl groups for covalent bonding to the methoxysilane groups of GOPS.[7] Two layers of the mixture were then spin-coated on samples for a total PEDOT:PSS thickness of approximately 250 nm (step iv). The top PaC layer was peeled off (step v). Finally, samples were hard-baked to crosslink PEDOT:PSS for one hour at 130 °C.

Prior to device characterization, samples were soaked in DI water overnight to remove any excess low-molecular weight additives from PEDOT:PSS. A polydimethylsiloxane (PDMS) well was attached to the gate and channel area of the sample and filled with 2 mL phosphate buffered saline (PBS). All electrical measurements were performed using a semiconductor device analyzer (Keysight B1500A) inside a Faraday cage under ambient conditions. After 5 minutes equilibrium time, a series of preconditioning cycles were carried out using a Ag/AgCl pellet (World Precision Instruments) as the gate electrode. As shown in Fig. S1(a) in the supplementary material, a series of 11 output cycles with V_G ranging from -0.5 to 0.5 V (0.1 V steps) and V_D ranging from -0.6 to 0.05 V (bidirectional) were performed. Next, a series of 5 transfer cycles with V_D stepping from -0.1 to -0.5 V and V_G ranging from -0.5 to 0.5 V were carried out, shown in Fig. S1(b) in the supplementary material. Immediately following the preconditioning cycles, transfer curves were measured with V_G ranging from -0.5 to 0.5 V at a fixed V_D of -0.4 V to simulate discrete measurements.

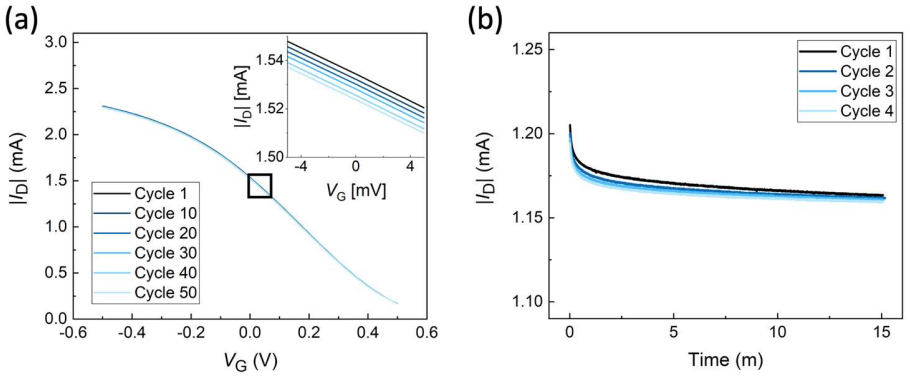

FIG. 2. (a) Transfer curves throughout 50 consecutive cycles, V_D = -0.4 V; (b) Four cycles of 15-minute continuous drain current measurement with 5 minute wait time between cycles, V_D = -0.4 V and V_G = 0.1 V.

For real-time measurements, I_D was measured after preconditioning cycling with a constant V_D of -0.4 V and V_G of 0.1 V, corresponding to the maximum g_m of these OECTs. I_D was measured for 15 minutes, followed by a 5 minute wait time. These continuous measurements were repeated 4 times for each OECT. To avoid PBS evaporation during real-time measurements, parafilm was placed over the PDMS well with only a small hole for the Ag/AgCl pellet, shown in Fig. S2 (supplementary material).

Fig. 1(b) shows an optical micrograph of the microfabricated PEDOT:PSS channel, where the channel width-to-length ratio (W/L) is 1 with a channel length of 50 µm determined by the gap between gold source and drain electrodes. Fig. 1(c) and 1(d) show a representative transfer curve and output curves of an OECT operated by a non-polarizable Ag/AgCl pellet as a gate electrode. A typical bell-shaped g_m curve plotted in red in Fig. 1(c) is observed with a maximum value of $g_{m.max} \approx 3.5$ mS at $V_G = 0.15$ V. The ON/OFF ratio, measured between V_G = -0.5 V and 0.9 V, was 63,500 (V_D = -0.4 V). For accurate measurements of analytes in discrete biosensing applications, cyclability of transfer curves are required. To test the cyclability, transfer curves were consecutively measured 50 times using a Ag/AgCl gate as shown in Fig. 2(a). These OECTs exhibits more than 99% I_D retention (0.7 % I_D reduction, Fig. S3, supplementary material) over 50 transfer curve cycles. This indicates good discrete stability for informing accurate medical decisions from analyte measurements by PEDOT:PSS OECT biosensors. Additionally, further cycling was performed on the same devices three months after fabrication. Similarly high current retention was measured with 1.01% I_D change after 50 cycles and 1.02% change after 100 cycles, shown in Fig. S4 (supplementary material). Furthermore, for continuous monitoring of analytes, minimal I_D drift is desired. To investigate the I_D drift, continuous

measurements were performed as shown in Fig. 2(b). I_D remained very stable, decreasing less than 1% after approximately two minutes stabilization time for each cycle. Initial stabilization time

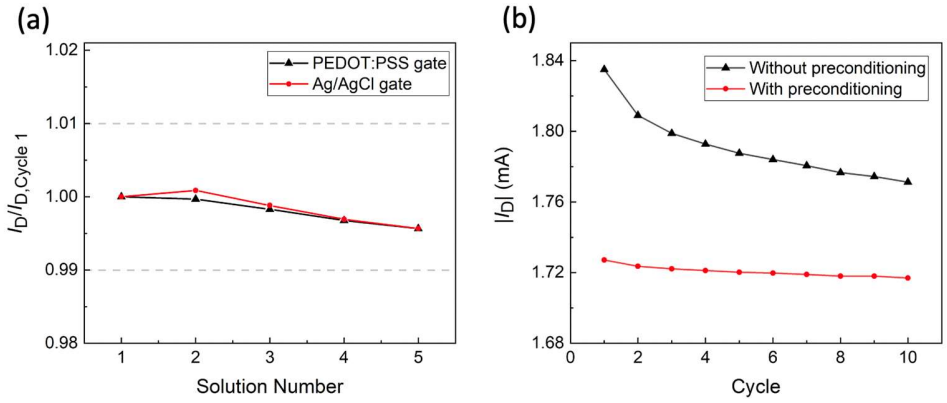

FIG. 3. (a) Drain current change for both PEDOT gated and Ag/AgCl gated OECTs with electrolyte mixing between cycles, V_D = -0.4 V and V_G = 0 V; (b) I_D change taken from 10 transfer curve cycles with V_D = -0.4 V and V_G = 0 V for an OECT before (black) and after (red) preconditioning cycling.

and small shifts between cycles should be accounted for in continuous biosensing applications. Outside of the initial stabilization time, the PEDOT:PSS OECTs show very minimal I_D drift.

In real biosensing applications, biofluids are continuously changed. In wearable sweat sensors, for example, new sweat is secreted and mixes with previously secreted sweat. This continuous change in biofluids is a potential source of baseline I_D drift which hinders accurate analyte measurements. To investigate the baseline I_D drift when changing biofluids, the transfer curves were recorded while changing PBS solutions. Specifically, after measuring the first transfer curve, 10% of the PBS solution was removed and replaced with fresh PBS. The solution was mixed by back-pipetting and a 5 minute wait time was given prior to measuring another transfer curve. This was repeated for a total of 5 solution changes. The I_D values were taken from V_G = 0 V and normalized to $I_{D,cycle1}$ which is I_D of the first cycle as shown in Fig. 3(a). The PEDOT:PSS OECT shows current retention within 1% even with changing electrolyte solutions.

In addition to the external Ag/AgCl gate, there are certain applications that require a planar gate architecture where biorecognition elements (such as enzymes) are attached on the gate electrode. To test the stability of the OECTs operated with a planar gate, transfer curves with changing electrolyte solutions were additionally measured with a large (3 x 3 mm^2) PEDOT:PSS gate fabricated next to the channel. The data represented by the black curve in Fig. 3(a) shows similarly high current retention to those with the Ag/AgCl gate. Additionally, continuous I_D was measured

using the planar PEDOT:PSS gate electrode using V_G = 0.3 V and V_D = -0.4 V corresponding to $g_{m,max}$ for the device. Similarly high current retention shown in Fig. 2(b) for the Ag/AgCl gated devices is exhibited by the PEDOT:PSS gated devices, shown in Fig. S5 (supplementary material). It should be noted that the $g_{m,max}$ for PEDOT:PSS gated devices shifts to a higher V_G than Ag/AgCl gated devices due to the work function difference.[24] These results suggest that PEDOT:PSS OECTs can be widely used for a host of biosensing applications using either the Ag/AgCl gate or the planar gate architecture.

We have found that there are three important considerations in maximizing OECT stability: using fresh GOPS, soaking in DI water, and device preconditioning. GOPS serves to crosslink PEDOT:PSS, rendering it insoluble in electrolyte and promoting adhesion to the substrate. Upon exposure to air, the silane and epoxide moieties hydrolyze and spontaneously crosslink. As shown in Fig. S6 (supplementary material), devices fabricated using old GOPS (from a bottle that has been used by multiple researchers over several months) are rather unstable, showing large transfer curve shifts with more than 15% I_D reduction after 5 transfer cycles. Therefore, it is vital to use freshly aliquoted GOPS from a tightly sealed container to ensure proper PEDOT:PSS crosslinking. Secondly, it is important to thoroughly soak devices in DI water before use. As indicated by previously reported contact angle measurements[25] PEDOT: PSS films continue to evolve in DI water throughout several hours of soaking as excess low molecular weight solvents are removed from PEDOT:PSS. Finally, the preconditioning output and transfer curve cycling is vital for achieving good stability. The effect of preconditioning is shown in Fig. 3(b), where the black curve represents I_D (V_G = 0 V) taken from 10 consecutive transfer curve measurements without prior preconditioning. After preconditioning cycling, transfer curves were repeated and exhibit more stable I_D throughout cycling, represented in red. As with soaking in DI water, we propose that the preconditioning step promotes the removal of the remaining low molecular weight compounds from the PEDOT:PSS. In summary, following the careful microfabrication protocol with special attention to GOPS freshness, PEDOT:PSS soaking, and preconditioning cycling will yield high quality OECTs suitable for rigorous biosensing applications, even with changing electrolyte solution.

This study demonstrated highly stable PEDOT:PSS electrochemical transistors for both discrete and continuous measurements. By following careful fabrication and preconditioning steps, 99% current retention was achieved using both non-polarizable Ag/AgCl and planar PEDOT:PSS gate electrodes. These transistor channels utilized commercially available PEDOT:PSS, allowing for facile fabrication and biocompatibility. In the case of discrete measurements, transfer curves were measured consecutively and remained stable throughout 50 cycles. Additionally,

transfer curve cycling was shown to be stable even after changing the electrolyte solution. To mimic continuous measurement techniques, drain current was measured for 4 cycles of 15 minutes with constant V_D and V_G. After an initial two minute stabilization period, minimal current drift was measured and only slight shifts occurred between cycles. These results suggest PEDOT:PSS electrochemical transistors could be used for commercialization in biosensing applications requiring highly stable cyclic discrete and continuous performance.

Supplementary Material

See supplementary material for the preconditioning cycling, testing setup, I_D over transfer curve cycling, PEDOT:PSS gated continuous measurements, and effect of GOPS freshness.

Conflicts of Interest

There are no conflicts to declare

Data availability

The data that support the findings of this study are available within the article and its supplementary material.

Acknowledgements

This work was supported by the Natural Environment Research Council (NERC) under award no. NE/T012293/1. S.L.B. acknowledges funding from the Cambridge International & Churchill Pochobradsky Scholarship.

References

[1]J. Rivnay, P. Leleux, M. Sessolo, D. Khodagholy, T. Hervé, M. Fiocchi and G. G. Malliaras, *Advanced Materials*, **25**, 7010–7014 (2013).

[2]D. Khodagholy, J. Rivnay, M. Sessolo, M. Gurfinkel, P. Leleux, L. H. Jimison, E. Stavrinidou, T. Herve, S. Sanaur, R. M. Owens and G. G. Malliaras, *Nature Communications*, **4**, 2133 (2013).

[3]J. Rivnay, P. Leleux, M. Ferro, M. Sessolo, A. Williamson, D. A. Koutsouras, D. Khodagholy, M. Ramuz, X. Strakosas, R. M.Owens, C. Benar, J. M. Badier, C. Bernard and G. G. Malliaras, *Science Advances*, **1**, e1400251 (2015).

[4]J. Rivnay, S. Inal, A. Salleo, R. M. Owens, M. Berggren and G. G. Malliaras, *Nature Reviews Materials*, **3**, 17086 (2018).

[5]M. J. Donahue, A. Williamson, X. Strakosas, J. T. Friedlein, R. R. McLeod, H. Gleskova and G. G. Malliaras, *Advanced Materials*, **30**, 1705031 (2018).

[6]M. Asplund, T. Nyberg and O. Inganäs, *Polymer Chemistry*, **1**, 1374–1391 (2010).

[7]A. Håkansson, S. Han, S. Wang, J. Lu, S. Braun, M. Fahlman, M. Berggren, X. Crispin and S. Fabiano, *Journal of Polymer Science Part B: Polymer Physics*, **55**, 814–820 (2017).

[8]D. Mantione, I. Del Agua, W. Schaafsma, M. Elmahmoudy, I. Uguz, A. Sanchez-Sanchez, H. Sardon, B. Castro, G. G. Malliaras and D. Mecerreyes, *ACS Applied Materials and Interfaces*, **9**, 18254–18262 (2017).

[9]S. Han, S. Yamamoto, A. G. Polyravas and G. G. Malliaras, *Advanced Materials*, **32**, 1–8 (2020).

[10]D. A. Koutsouras, K. Lieberth, F. Torricelli, P. Gkoupidenis and P. W. Blom, *Advanced Materials Technologies*, 2100591 (2021).

[11]H. Tang, F. Yan, P. Lin, J. Xu and H. L. Chan, *Advanced Functional Materials*, 2011, **21**, 2264–2272. 12 C. Liao, M. Zhang, L. Niu, Z. Zheng and F. Yan, *Journal of Materials Chemistry B*, **1**, 3820–3829 (2013).

[12] C. Liao, M. Zhang, L. Niu, Z. Zheng and F. Yan, Journal of Materials Chemistry B, 1, 3820–3829 (2013).

[13]A.-M. Pappa, V. F. Curto, M. Braendlein, X. Strakosas, M. J. Donahue, M. Fiocchi, G. G. Malliaras and R. M. Owens, *Advanced Healthcare Materials*, **5**, 2295–2302 (2016).

[14]C. Diacci, J. W. Lee, P. Janson, G. Dufil, G. Méhes, M. Berggren, D. T. Simon and E. Stavrinidou, *Advanced Materials Technologies*, **5**, 1900262 (2020).

[15]W. Hai, T. Goda, H. Takeuchi, S. Yamaoka, Y. Horiguchi, A. Matsumoto and Y. Miyahara, *Sensors and Actuators, B: Chemical*, **260**, 635–641 (2018).

[16]K. Guo, S. Wustoni, A. Koklu, E. Díaz-Galicia, M. Moser, A. Hama, A. A. Alqahtani, A. N. Ahmad, F. S. Alhamlan, M. Shuaib, A. Pain, I. McCulloch, S. T. Arold, R. Grünberg and S. Inal, *Nature Biomedical Engineering 2021 5:7*, **5**, 666–677 (2021).

[17]N. Saraf, E. R. Woods, M. Peppler and S. Seal, *Biosensors and Bioelectronics*, **117**, 40–46 (2018).

[18]Y. Liang, C. Wu, G. Figueroa-Miranda, A. Offenhäusser and D. Mayer, *Biosensors and Bioelectronics*, **144**, 111668 (2019).

[19]D. A. Bernards and G. G. Malliaras, *Advanced Functional Materials*, **17**, 3538–3544 (2007).

[20]H. Y. Y. Nyein, M. Bariya, B. Tran, C. H. Ahn, B. J. Brown, W. Ji, N. Davis and A. Javey, *Nature Communications 2021 12:1*, **12**, 1–13 (2021).

[21]M. Moser, T. C. Hidalgo, J. Surgailis, J. Gladisch, S. Ghosh, R. Sheelamanthula, Q. Thiburce, A. Giovannitti, A. Salleo, N. Gasparini, A. Wadsworth, I. Zozoulenko, M. Berggren, E. Stavrinidou, S. Inal and I. McCulloch, *Advanced Materials*, **32**, 2002748 (2020).

[22]S.-M. Kim, C.-H. Kim, Y. Kim, N. Kim, W.-J. Lee, E.-H. Lee, D. Kim, S. Park, K. Lee, J. Rivnay and M.-H. Yoon, *Nature Communications 2018 9:1*, **9**, 1–9 (2018).

[23]A. G. Polyravas, V. F. Curto, N. Schaefer, A. B. Calia, A. Guimera-Brunet, J. A. Garrido and G. G. Malliaras, *Flexible and Printed Electronics*, **4**, 044003 (2019).

[24]S. Han, A. G. Polyravas, S. Wustoni, S. Inal, and G. G. Malliaras, *Adv. Mater. Technol.*, **6**, 2100763 (2021).

[25]C. Duc, A. Vlandas, G. G. Malliaras and V. Senez, *Soft Matter*, **12**, 5146–5153 (2016).